UNIVERSITY OF CALIFORNIA,
IRVINE

Silica nanoparticle platform to generate new molecular probes for fluorescence lifetime imaging

THESIS

submitted in partial satisfaction of the requirements
for the degree of

MASTER OF SCIENCE

in Biomedical Engineering

by

Soo Young Song

Thesis Committee:
Assistant Professor Jered B. Haun, Chair
Assistant Professor Michelle A. Digman
Assistant Professor Allon I. Hochbaum

2016

TABLE OF CONTENTS

LIST OF FIGURES

LIST OF TABLES

ACKNOWLEDGMENTS

I would first like to thank my committee chair, Professor Haun. Throughout the years of my undergraduate and graduate careers, the door to Prof. Haun's office was always open whenever I ran into a problem or had a question about my research and writing. He steered me in the right direction whenever he thought I needed it, and his intellectual ability to tackle a trouble spot from different angles continually inspired me to become a better researcher. Without his guidance, persistent help, and patience, this thesis would not have been possible. I would also like to thank my committee members, Professor Digman and Professor Hochbaum, who have been supportive in getting through this process.

In addition, I would like to acknowledge Laser Spectroscopy Facility for Dynamic Light Scattering measurements. Scattering Electron Microscopy (SEM) work was performed at the UC Irvine Materials Research Institute (IMRI), using instrumentation funded in part by the National Science Foundation Center for Chemistry at the Space-Time Limit (CHE-082913). Also, the fluorescence emission readings and Fluorescence Lifetime Imaging Microscopy (FLIM) experiments reported in this thesis were performed at the Laboratory for Fluorescence Dynamics (LFD) at UC Irvine. The LFD is supported jointly by the National Institutes of Health (8P41GM103540) and UCI. Also a special thank you to HongTao Chen for providing consultation for FLIM data acquisition and analysis, Dr. Zheng and Kenta Ohtaki for helping me when I ran into a trouble spot during SEM imaging, and Tyson Patros at Graduate Resource Center for writing consultations.

Finally, I must express my profound gratitude to Rajesh Kota and Sumi Lee for helping me to grow as a better researcher by sharing their knowledge and laboratory experience/skills with me, and all of those who work in Haun lab for making the lab environment enjoyable.

ABSTRACT OF THE THESIS

Silica nanoparticle platform to generate new molecular probes for fluorescence lifetime imaging

By

Soo Young Song

Master of Science in Biomedical Engineering

University of California, Irvine, 2016

Assistant Professor Jered B. Haun, Chair

Fluorescence microscopy is the most widely used detection method to image molecular probes, but is currently hindered due to the limited number of fluorescent probes available. The fluorescence lifetime of fluorescent probes that is the time an excited fluorophore takes to return to the ground state; this thesis studied a novel system to manipulate the fluorescent molecules' lifetime using the nanoprobe format. This system can exponentially increase the number of fluorescent probes. The first part of this thesis reports ~130nm silica nanoparticles labeled with silanized fluorescent dyes – Oregon Green 488, BODIPY, and rhodamine – using various total dye loadings. As the total dye loading increased, the relative fluorescence efficiency decreased due to self-quenching. This self-quenching effect was characterized by the phasor approach to fluorescence lifetime that gave unique and distinguishable spatial values of the nanoparticles. Utilizing the synthetic versatile properties of silica in accommodating other materials, the second part of this thesis discussed core-shell structured silica nanoparticles with an independent control to the fluorescence lifetimes of the cores and the shells. 35nm Silica cores were synthesized using a reverse microemulsion method. Various concentrations of fluorescent

nanomaterials encapsulated inside the cores govern the cores' phasor values. Subsequently, silica shells with various thicknesses were synthesized using the Stober sol-gel reaction. Various total dye loadings govern the shells' phasor values while the shell thicknesses control their fluorescence intensity. The distinct fluorescence lifetime phasor values enable nanoprobes to have visually effective representations that can be easily expanded by simply manipulating the molecular proximities between fluorophores.

CHAPTER 1. INTRODUCTION

1.1 Molecular detection, targeted drug delivery, and nanoparticles

Human cells maintain their functions and formations through a complex and interconnected molecular system. When regulated cell growth and normal molecular activity is disrupted, chronic diseases such as cancer and cardiovascular disease occur [1, 2]. Furthermore, tumors tend to be extremely dynamic and heterogeneous [3]. However, the current cancer diagnostics and therapeutic treatments are capable of neither fully recognizing these unique molecular characteristics nor distinguishing them from those of normal cells. On the other hand, molecular probes and drug carriers can selectively and specifically detect these unique molecular expressions through affinity ligands and bioconjugation techniques. Due to the selective targeting ability of molecular probes and drug carriers, their development in molecular detection and targeted drug delivery may drastically increases diagnostic sensitivity as well as therapeutic specificity and efficacy.

The nanoparticle (NP)-based molecular targeting is an excellent system for this purpose as they offer high drug loading capacity, protection, multivalent targeting capability, and tunable physical properties [4, 5]. Therapeutic agents can be assigned to NPs by various methods such as entrapment, adsorption, attachment and encapsulation of drug [6]. Because NPs have a high surface-volume ratio, drugs can be loaded with high loading efficiency. Once the external surface of NPs is functionalized with site-specific targeting molecules, the NPs bind to the target area and provide a sustained drug release of therapeutic agents. The surface of the NPs can also have multivalent targeting abilities to enhance binding to target receptors. Moreover, when the NPs encapsulate therapeutic agents and fluorescent tags, the NPs provide an effective protection of the agents against enzymatic degradation and the tags against photodegradation [7, 8]. The

ease of size control, varying from tens of nanometer to a micrometer scale, makes the NPs favorable to pharmacokinetics as well [9, 10]. NPs bear multifarious advantageous traits for biomedical nanotechnology and are a very effective means to support molecular diagnosis and treatment.

1.2 Silica nanoparticles

Drug carriers and detection nano-probes have been developed utilizing a broad range of nanomaterials, such as polymer, magnetic, gold, and quantum dots. However, these nanomaterials often suffer from limitations, including poor biocompability, high toxicity, complicated external stimuli setup and rapid elimination due to the immune system [11]. For example, magnetic particles require external magnetic fields that are deep enough to penetrate the target site while maintaining a balanced focus and intensity [12]. The complicated external stimuli make these particles difficult to apply in vivo. Polymer particles are biodegradable, but their hydrophobic properties suffer from poor administrations of hydrophilic drugs and molecules [13]. Meanwhile, cytotoxicity and fluorescence intermittency hinder in vivo studies of quantum dots that often require a secondary coating or shell.

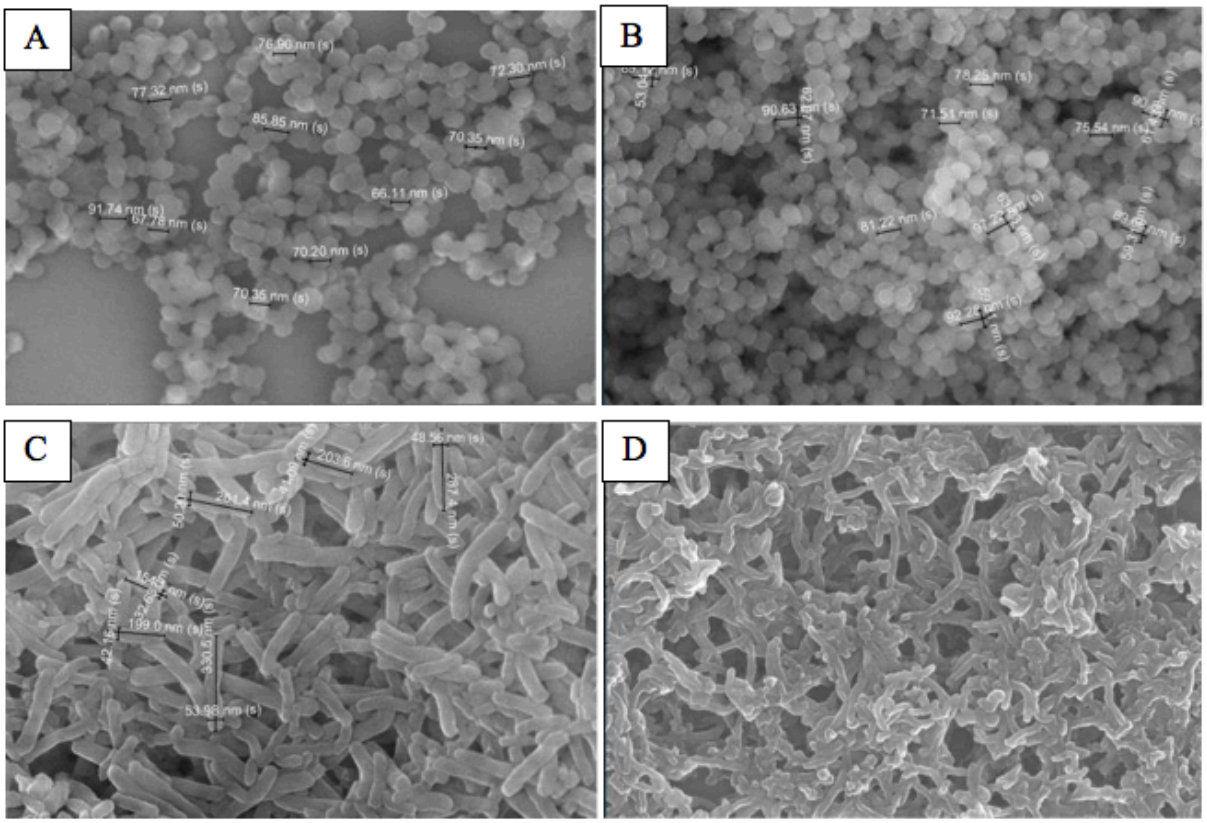

Figure 1 | Scanning electron microscope images of silica nanoparticles in various shapes from spheres (A) and short rods (B) to elongated rods (C, D) [23]. Size and shape of silica nanoparticles synthesized in Stober sol-gel reaction can be easily controlled by simply varying the concentrations of catalysts and surfactants.

Silica NPs and silica-coated NPs, on the other hand, exhibit unique characteristics and advantages to overcome these limitations. The stability of these NPs in aqueous solutions and their biocompatibility make them excellent nanomaterials for molecular diagnostics and treatments. In vivo studies have demonstrated that silica NPs are relatively biocompatible as they have shown a minimum effect on cell survival when introduced into cells [14]. Silica NPs also have demonstrated negligible level of toxicity along with desirable pharmacokinetic characteristics when executed in a moderate dose [14, 15]. On top of innate properties such as biocompatibility and pharmacokinetics, high control size and shape and its easiness are another

important elements of silica NPs in the development of molecular targeting systems (See *Figure 1*). The physical design parameters determine cellular uptake, targeting efficiency, and bio-distribution of nanoparticles, and may also affect drug release dynamics to the target site [6]. Furthermore, silica is very compatible with other nanomaterials, such as magnetic, quantum dots, and gold, and can act as an excellent protector when used as an encapsulating material, improving cytotoxicity, shelf life, and drug administration [16]. Consequently, this synthetic versatile properties of silica has attracted a great amount interest in silica NPs.

1.3 Fluorescence lifetime imaging for extreme multiplexing

Multiplexed molecular diagnostics is a rapidly growing field that can simultaneously obtain more information from a single sample by increasing the number of detection channels. The most common biological detection method for molecular configuration is fluorescence microscopy [17]. Using this method, NPs or molecules can be labeled with different fluorescent probes that have distinguishable excitation and emission from each other. Fluorescent labeling enables each type of detection channel to represent unique information about a sample. However, increasing the number of detection channels is currently hindered due to the limited number of fluorescent probes available that have distinguishable excitation and emission signals in the conventional intensity-based fluorescence imaging.

In addition to utilizing the conventional fluorescent properties, manipulating their fluorescence lifetime can not only conquer the obstacles of the conventional method of characterizing detection probes but also can exponentially increase the number of the detection channels. Fluorescence lifetime is the time a fluorophore takes to return in its ground state from the excited state, which depends on both radiative and non-radiative energy process. Thus,

manipulating the ratios of of radiative and non-radiative components of a single type of fluorescent probe gives an exponential rise in the number of detection tags that are unique and distinguishable by fluorescence lifetime. One way to manipulate the ratios is self-quenching by varying the close proximity of fluorescent molecules. Self-quenching occurs when the distance between fluorophores are closer than the distance range where fluorescence resonance energy transfer (FRET) occurs. In a self-quenched environment, the excited energy of a donor fluorophore gets deactivated instead of getting transferred by a neighboring molecule. A combination of radiative emission, and non-radiative energy transfer, and non-radiative energy deactivation influence how the fluorophores response to a frequency-modulated laser and can be interpreted by a phasor approach to fluorescence lifetime imaging microscope (FLIM). This approach provides graphical representations of the NP characterization on a phasor plot and provides a powerful tool to expand the detection probe library. Using the phasor approach to expand the library is not limited to NPs labeled with homogenously populated fluorescent dye molecules. This approach can also extend to NPs involving multiple nanomaterials of different lifetimes in various NP structures.

1.4 Project overview

The first part of this thesis work will focus on fluorescence analyses on spherical silica NPs synthesized by Stober sol-gel method. The Stober sol-gel method was chosen for this part of study, as it provides high control over size, and simplicity in synthesis system and fluorescent labeling. In order to demonstrate a system that can increase the number of detection channels for multiplexing molecular detection system, this thesis will perform a characterization of fluorescence lifetime of NPs via phasor method in addition to fluorescence absorption and

emission analyses. The variation of fluorescence lifetime in the silica NPs employs fluorescence self-quenching mechanism by covalently incorporating silanized fluorescent dyes (Si-F) into the silica matrix. FLIM will then detect unique phase shifts and modulation depths with a modulated light source and a modulated detector, and interpret the acquired data into phasor plots.

Carrying out the same concept, the second part of the work will discuss how multiple nanomaterials of different fluorescence lifetimes in a single NP can also support the expansion of the detection probe library. To exemplify this application, silica NPs with core-shell structure will be examined. The ~35nm cores will be synthesized using a reverse microemulsion method, and the shells with various thicknesses are going to be added onto the cores in a Stober sol-gel reaction. This thesis will report the characterization of the core size and the shell thickness and will present a system that can independently manipulate the fluorescence lifetimes of the cores and the shells through the phasor approach. The fluorescence lifetime of the shells is governed by the total dye loading to the silica matrix. The silica cores can potentially encapsulate various nanomaterials that their fluorescence lifetimes can be manipulated by varying the concentrations of the nanomaterials inside the cores. To exemplify this concept, QD-encapsulated silica (QD-Si) cores—fluorescent silica shell NPs were chosen to demonstrate a system with the independent fluorescence lifetime control of the cores and the shells, and how that contributes to the expansion of the detection channel library.

CHAPTER 2. PHASOR APPROACH TO FLUORESCENCE LIFETIME OF SILICA NANOPARTICLES

2.1 Background

i) Stober sol-gel synthesis

In 1968, Stober *et al*. introduced sol-gel reaction that creates homogeneous spherical silica particles in different sizes with continuous hydrolysis and condensation in alcoholic solvent [18]. The process involves tetraethylorthosilicate (TEOS) catalyzed by mineral acid or base. Silanol groups are formed from hydrolysis of TEOS. The silanol groups then go through condensation, which create siloxane groups (Si—O—Si) that are a basis of silica matrix. Stober also reported that concentration of ammonia and types of alcoholic solvents in reaction solution are determining factors to the particle size. Stober's work became the basis for scientists to develop more systematic synthesis methods. Bogush *et al*. achieved silica nanoparticles ranging from 40nm to few micrometers in diameter by varying concentration of ammonia, types of solvent, and reaction temperature [19]. Due to its simple and effective synthesis system for size control, and ability to easily scale up for mass production, Stober sol-gel reaction has become one of the most studied methods to synthesize silica NPs. Moreover, researchers have used the high control over size and shape of Stober synthesis method to investigate the effects of the various design parameters of NPs on the adhesion kinetics in targeted delivery systems, such as multivalent targeting and hydrodynamic force effects under vascular flow [20].

ii) Fluorescence labeling for multiplexing molecular detection

Fluorescence lifetime is the average time for a molecule takes to emit a photon from the excited state. A photon can return to its ground state via radiative or non-radiative emissions. The intensity of fluorescent emission increases as fluorophore concentration increases until it reaches a critical concentration. When the concentration of fluorophores exceeds the critical concentration, an excited fluorescent molecule non-radiatively transfers the energy to the nearby fluorophores without emitting photons due to FRET. At higher concentrations, however, a fluorophore experiences self-quenching due to contact between fluorophores or between a fluorophore and another molecule, such as oxygen, halogen, and amine [21]. This contact decreases the fluorescence intensity because a contact of another molecule with a fluorophore non-radiatively *returns* the energy of the excited fluorophore to the ground state rather than non-radiatively *transfering* the energy as FRET. As the contact of another molecule deactivates the excited state, fluorescence intensity is no longer proportional to the concentration of the fluorophores, and exhibits collisional quenching behaviors [21]. The relationship between fluorescence intensity and fluorophore concentration is described by Stern-Volmer equation:

$$I_0/I = 1 + K_{SV}[Q] = 1 + K_q\tau_0[Q]$$

where I_0 is an intensity without molecular contacts to fluorophores, K_{SV} is Stern-Volmer quenching constant, [Q] is concentration of quencher, K_q is biomolecular quenching rate constant, and τ_0 is a lifetime in the absence of quencher. I_0/I is proportional to [Q] because increasing [Q] creates more probability of the molecular contact, thus further decreasing the

intensity via non-radiative energy deactivation. When the system is purely based on collisional quenching, the following equation applies:

$$I_0/I = \tau_0/\tau$$

Therefore a general relationship between concentration, lifetime, and intensity is that an increase in concentration is responsible for a decrease in lifetime and intensity.

While time domain lifetime can gauge the level of self-quenching, frequency domain lifetime reveals additional information that brings essential elements of phasor approach to fluorescence lifetime. Instead of a pulse of light as an excitation source in time domain, an intensity-modulated sinusoidal light excites a fluorescent sample in frequency domain. A delay between the point of excitation and the response of the fluorophores to the stimuli is measured by phase shift (φ) and modulation amplitude (M). A coordinate derived from φ and M provides its vectorial representation on a phasor plot while the x-coordinate being $M\cos\varphi$ and the y coordinate being $M\sin\varphi$. The phasor-interpreted fluorescence lifetime is a convenient approach to mark multiplexing probes as they provide a visual display to characterize each detection channel.

In this part of the present work, the fluorescence quenching was demonstrated in silica NPs by covalently incorporating Si-F into the silica matrix synthesized in Stober sol-gel reaction. NPs were labeled with different Si-F such as BODIPY, rhodamine, and Oregon Green 488 with different fluorescent dye-to-aminosilane (F:Si) molar ratios to manipulate phasor values of fluorescence lifetime. Note that the NPs were synthesized in spheres, and their average size was kept consistent to 130nm in diameter for the fluorescence analyses to simplify the experimental design while maintaining uniformly populated particles. Any fluorescent phase shifts and changes in modulation depths were detected with a modulated light source of FLIM, whose software then generated vectorial representations of the collected data on a phasor plot.

2.2 Materials and methods

i) Nanoparticle synthesis

For the control sample, 1.2ml of strong ammonia solution (26° Baume, Fisher Scientific; will be referred to as ammonia) was added to 18ml of ethanol. Simultaneously, 500ul of tetraethyl orthosilicate (TEOS, 98%, Sigma-Aldrich) and a solution containing Si-F (from *part ii*) were slowly added to the mixture while vigorously stirring. The solution was being kept stirred at room temperature overnight. Dispersion of the particles in ethanol and water were made by successive centrifugation and replacement of supernatant. (@ 1200 rpm, 3 min for each round of wash).

ii) Fluorescence labeling

3-aminopropyl trimethoxysilane (APTS, 97%, Sigma-Aldrich) and three amine-reactive fluorescent dyes were used to synthesize fluorescent labels. Each of the following dyes: 5-(and 6)-carboxytetramethylrhodamine succinimidyl ester (NHS-Rhodamine, Thermo Scientific; will be referred to as rhodamine), BODIPY TMR-X NHS succinimidyl ester (Thermo Fisher Scientific; will be referred to as BODIPY), or Oregon Green 488 carboxylic acid, succinimidyl ester, 6-isomer (Thermo Fisher Scientific; will be referred to as Oregon Green) was coupled with various amounts of APTS (1ul, 5ul) and different F:Si molar ratios (1:300, 1:100, 1:30, 1:10) in 2ml of ethanol under stirring in dark for 24 hours. The Si-F and TEOS are then simultaneously added to particle synthesis solutions in order to co-condensate dyes into the silica matrix (refer to *part i*).

iii) Characterization of nanoparticles

Size of nanoparticles

Diameters of spherical particles were collected by dynamic light scattering (Malvern Zetasizer ZS Nano DLS). The samples were prepared by dispersing particles into 1ml of water. The angle of detection was set to 175° backscatter.

Fluorescence Absorption and Emission

Changes in fluorophore concentration-dependent absorption and emission intensities were recorded by NanoDrop 2000 UV-Vis Spectrophotometer (Thermo Scientific) and FluoroMax-4 Spectrofluorometer (Horiba Scientific) respectively. The samples kept the concentration consistent throughout the measurements at approximately 0.3nM (refer to *Appendix A* to see the calculation for the concentration). The range of absorption reading was set to 480-500nm, 540-560nm, 535-550nm, and the emission peak was set to 524nm, 575nm, 573nm for Oregon Green NPs, rhodamine NPs, and BODIPY NPs, respectively. The slit for the monochromator was set to 5nm.

Fluorescence Lifetime

The phasor approach to fluorescence lifetime imaging analysis was performed by Olympus FluoView FV1000 with IX81 microscope. The excitation wavelength of the laser was set to 405nm/488nm, 405-440nm/515nm, 488nm/543nm/633nm, and the emission detection range was set to 505-605nm, 560-660nm, 575-675nm for Oregon Green NPs, rhodamine NPs, and BODIPY NPs, respectively. All the measurements were referenced to Rhodamine 110 dye. All measurements consisted of a minimum 100 photon counts in order to obtain reliable phasor fluorescence lifetime distributions.

2.3 Results and discussion

i) Nanoparticle synthesis: Size analysis

To understand the effects of ammonia concentration on particle formation, different amounts of ammonia were used in the particle synthesis solutions: 0.8ml, 1ml, 1.2ml, and 1.4ml. The rest of the reagents was kept constant. DLS measured the particle diameters through the Stokes-Einstein equation using the speed of the Brownian motion of the particles in water. The result showed that the diameters of particles increase as the amount of ammonia increases: 40nm, 71nm, 126nm, and 213nm in diameter for 0.8ml, 1ml, 1.2ml, and 1.4ml of ammonia, respectively.

DLS also determined the size of fluorescent dye-conjugated NP samples synthesized with 1.2ml ammonia. Oregon Green-labeled particles were 154 ± 30nm in diameter, 117 ± 10nm for rhodamine-labeled particles, and 109 ± 21nm for BODIPY-labeled particles. Slightly bigger diameters were shown in the samples that used 5ul APTS than those that used 1ul APTS by 8.8nm in average. Increasing the amount of aminosilane used for Si-F reaction may have provided more silane molecules that can be covalently incorporated to the silica particle matrix, thus the increase in particle volume.

ii) Fluorescence Analysis

Before adding aminosilane-conjugated fluorescent dyes to the particle synthesis solution, Si-F solutions were tested with thin layer chromatography (TLC) to see the reaction has gone to completion. Free aminosilanes were still present in the solution, which was expected due to a molar excess of aminosilane in the Si-F reaction system. These free aminosilanes become important for surface characterization in a post-modification process. When the free aminosilane molecules are incorporated into the silica particle matrix, the particle surface expresses a part of

the amine groups. During the post-modification process, they can be selectively functionalized with bioconjugating molecules for site-specific targeting purposes. On the other hand, all the dye molecules theoretically should have been reacted, but TLC tests indicated that there was a small amount of unreacted fluorescent dyes in Si-F solution. The hydrophobic properties of the dyes in hydrophilic solutions may have been a possible cause for unreactivity between the dye molecules and aminosilanes acting against the amine reactivity of the dyes to aminosilane [23].

During the synthesis for fluorescent silica nanoparticles, the reaction mixture was observed as opaque pastel pink for particles labeled with rhodamine and BODIPY and light pastel yellow for particles with Oregon Green. Increasing the amount of aminosilane in the Si-F reaction intensified the color. In the case of rhodamine and BODIPY, the color darkened to turbid reddish purple, and Oregon Green sample turned from light pastel yellow to cloudy yellow.

The precipitates after centrifugation were pink or purple for rhodamine and BODIPY, and yellow or yellowish orange for Orgeon Green depending on the F:Si ratios and the amount of aminosilane used. During the first few washes, the supernatant after centrifugation was colored, indicating that not all APTS-coupled fluorophore molecules are incorporated into the silica nanoparticle matrices. A possible explanation for the free APTS-coupled dyes in the supernatant is the different reaction rates of TEOS and APTS. Not only that TEOS has a hydrolysis rate that is five times faster than that of APTS but also siloxane bonding between TEOS molecules is much faster than hydrolysis [24]. Pre-hydrolyzing silanized fluorophores with catalyst

beforehand would have been a solution to this issue. However, possible formations of fluorophore dimers or oligomers may result in an unequal distances or contacts between fluorophores in a silica matrix, thus a non-homogenous population of particles in terms of self-quenching.

Fluorophore concentration-dependent absorption and emission intensities were recorded by UV-Vis spectrophotometer and spectrofluorometer. As the concentration of fluorophores increases, fluorophores and other molecules in close proximity eventually come into a contact. A molecular contact with fluorophores induces a non-radiative energy deactivation, and the fluorescent signal loss reduces intensities of absorption and emission. In *Table 1*, fluorescence absorption and emission intensity, and relative fluorescence efficiency are shown. Since UV-Vis spectrophotometer automatically referenced fluorescence absorption readings off of the absorption of intensity of silica matrix, the absorption intensity profile curves and the maximum intensity values differed depending on the size and the make-up of the particles (e.g. different amounts of amines). Therefore, fluorescence absorption and emission intensities were normalized respect to absorption intensities of the silica matrix. The silica intensity spectra were observed approximately from 250nm to 300nm, so the intensity values were measured at 280nm.

[Oregon Green-labeled silica nanoparticles]

Sample	TEOS Absorption (1mm path.)	Oregon Green Absorption (1mm path.)	Normalized Absorption	Oregon Green Emission (mV)	Normalized Emission	Relative Fluorescence Efficiency
1:300 & 1ul	1.227	0.231	0.19	9.58×10^6	7.81×10^6	3.4
1:30 & 5ul	1.373	0.468	0.34	1.68×10^7	1.22×10^7	3.0
1:10 & 5ul	0.991	0.668	0.67	8.09×10^6	8.16×10^6	1

[Rhodamine-labeled silica nanoparticles]

Sample	TEOS Absorption (1mm path.)	Rhodamine Absorption (1mm path.)	Normalized Absorption	Rhodamine Emission (mV)	Normalized Emission	Relative Fluorescence Efficiency
1:100 & 1ul	1.06	0.14	0.13	5.64×10^6	5.32×10^6	58.7
1:30 & 5ul	1.25	0.42	0.34	3.47×10^6	2.78×10^6	12.0
1:30 & 1ul	0.692	0.49	0.71	2.39×10^6	3.45×10^6	7.1
1:10 & 5ul	1.18	0.78	0.66	5.36×10^5	4.54×10^5	1

[BODIPY-labeled silica nanoparticles]

Sample	TEOS Absorption (1mm path.)	Bodipy Absorption (1mm path.)	Normalized Absorption	Bodipy Emission (mV)	Normalized Emission	Relative Fluorescence Efficiency
1:300 & 1ul	0.915	0.106	0.12	4.25×10^6	4.64×10^6	24.2
1:30 & 1ul	0.756	0.112	0.15	1.12×10^7	1.48×10^7	60.2
1:10 & 1ul	0.482	0.137	0.28	9.47×10^6	1.96×10^7	41.6
1:30 & 5ul	0.899	0.261	0.29	8.38×10^6	9.32×10^6	19.3
1:10 & 5ul	0.886	0.598	0.67	9.94×10^5	1.15×10^6	1

Table 1 | Intensity readings of fluorescence absorption and emission of silica nanoparticles labeled with Oregon Green, rhodamine, and BODIPY. Note that 1) samples are indicated by their F:Si molar ratios & the amounts of aminosilane used for the dye coupling reaction. 2) TEOS absorption intensity readings were obtained at 280nm. 3) Both absorption and emission intensities were normalized respect to absorption intensity of silica matrix.

As can be seen in *Table 1*, relative fluorescence efficiency decreased as the amount of aminosilane or F:Si ratio increased, indicating that quenching of fluorescent molecules has taken place in the particles. BODIPY-labeled 1:300 & 1ul sample showed a relatively low fluorescence efficiency considering the minimum amount of aminosilane and the F:Si ratio low enough for the fluorescent molecules to fluoresce without a significant non-radiative deactivation. This might have been a result of a high noise-to-signal ratio due to the low concentration of the dye interfering an accurate reading of the maximum absorption intensity. Also note that absorption peaks were red-shifted ~10nm as spectra of aggregated dye molecules tend to deviate from wavelength-dependent Lambert-Beer Law behavior [25]. Spectral red-shift of absorption in aggregated dye molecules is a phenomenon attributed to transitions to the lower energy state of non-monomer than that of the respective monomer molecules [26].

Phasor approach to fluorescence lifetime imaging analysis was demonstrated with FLIM. The main parameter that contributed to self-quenching was the concentration of fluorophores and aminosilane. In this particular experimental design, the amount of aminosilane and the F:Si ratios were the determining factors for the level of self-quenching in the fluorescent NPs.

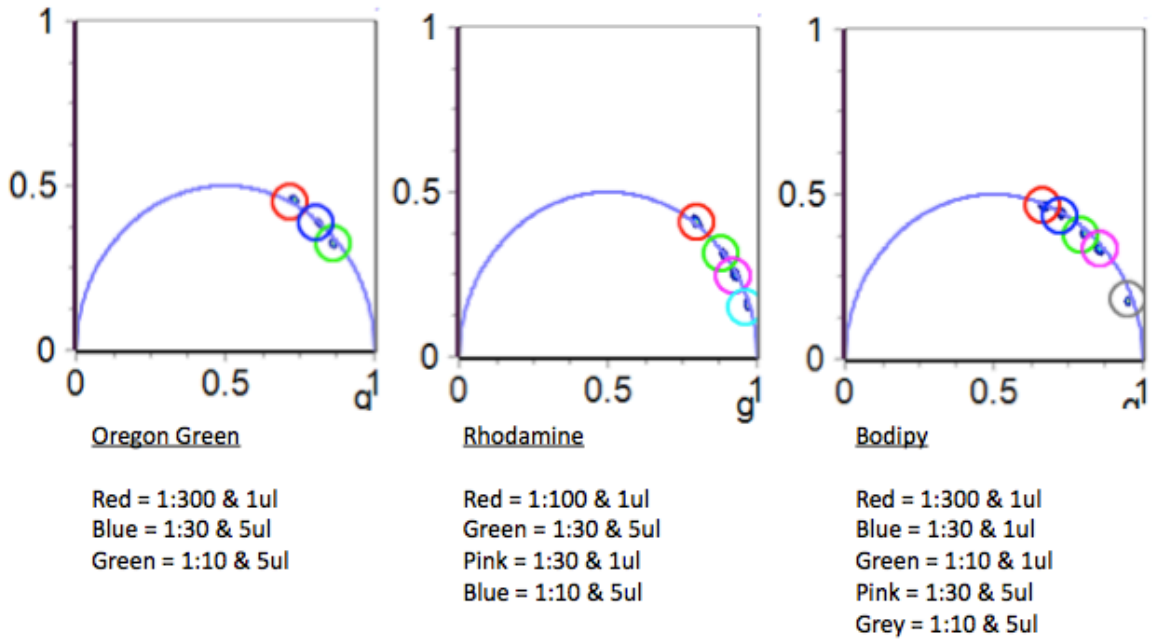

Figure 2 | Phasor plots of fluorescence lifetime of the silica NPs labeled with different fluorescent dyes, F:Si ratios, and the amount of aminosilane. The three plots are in the following order: Oregon Green, rhodamine, and BODIPY labeled silica NPs. Each colored circle marks a phasor point of a NP sample with a F:Si ratio and a amount of aminosilane described below each plot.

The variation of quenching only occurred along the universal circle of phasor plots since the NPs consisted of a homogeneous population of fluorophores (*Figure 2*). As expected, the NPs showed an increasing level of quenching and shortening of lifetime as the amount of aminosilane or the F:Si ratios increased.

This part of the thesis work synthesized ~130nm spherical silica NPs labeled with three different fluorescent dyes. The fluorescence analysis successfully demonstrated that the particles with the same excitation and emission wavelengths can exhibit various fluorescence lifetime through phasor approach by manipulating molecular proximity of fluorophores and non-radiative process of self-quenching.

CHAPTER 3. SILICA NANOPARTICLES WITH CORE-SHELL ARCHITECTURE

3.1 Background

The need to develop nanomaterials with more complex architecture that is multifunctional yet biocompatible has driven researchers to explore various designs of NPs consisting of multiple materials. One of the NP designs that has attracted great interest is NPs with core-shell architecture, usually the shells consisting of more biocompatible and other inorganic materials. One of the widely used materials creating the shell, which will create the cores, is silica. Silica is biocompatible, versatile in accommodating foreign materials, and versatile for surface functionalization due to its silanol groups [27]. Having a silica shell as a protective layer also provides protection of fluorescent molecules from photodegradation and therapeutic drugs from enzymatic degradation. Overall, a silica shell acts as a supplement to make up for the limitation of the encapsulated materials or as a mediator between the bioenvironmental system and those materials to enhance functionality and imaging efficiency of the NPs. For example, gold NPs have intense absorption and light scattering due to the surface pasmon resonance (SPR), and gold core-silica shell NPs can tune the SPR by adjusting core to shell ratio to obtain optimal imaging results [28]. Adding silica layer to iron oxide NPs mitigates agglomeration, resulting in better biodistribution and longer retention time in the blood circulatory system [27].

Another advantage of combining various nanomaterials and silica in a core-shell structure is an ability to expand the detection probe library even more than the system presented in *Chapter 2*. When the fluorescent dye labeling in the silica shell matrix combines with the unique fluorescent properties of nanomaterials in the silica cores, the core-shell NPs can contribute to

the expansion of the detection probe library using a phasor approach to fluorescence lifetime. The phasor interpretations give a graphical representation of the lifetime of the core-shell NPs. In this graphical representation, their relative distances between the distinct phasor values of the nanomaterials encapsulated in the cores and the fluorophores in silica shell matrix appears on a junction depending on their relative populations of the two components. Therefore, theoretically, a combination of the two components will yield multi-exponential decay appearing inside the universal circle that gives another parameter to manipulate the fluorescence lifetime of the NPs on a phasor plot. Integrating with fluorophore labeling into silica core-shell NPs provides multiple parameters to control phasor distribution of detection channels and to expand the multiplexing bioanalysis probe library.

This thesis presents a system to synthesize silica core-silica shell NPs: the cores are synthesized through a reverse microemulsion, which is adapted from Darbandi *et al.*, and fluorescently labeled silica shell are synthesized through a Stober sol-gel method [29]. This novel system includes the following significant parameters: the lifetime of the nanomateirals in silica cores, and the various thicknesses and fluorescence lifetimes silica shells. Varying the thickness of the silica shells is to control fluorescence intensity of the shells. As performed in the pervious fluorescence labeling protocol in *Chapter 2*, varying the fluorescence lifetime of the fluorescently labeled silica matrix by changing the amounts of aminosilanes and F:Si ratios is to govern the degree of quenching among fluorophores in the silica shell. Varying the lifetime of the nanomaterials in the silica cores gives the core-shell NPs an additional parameter to control their fluorescence lifetime. This allows the independent control of the fluorescence lifetime of nanomaterials in silica cores and fluorescent dyes in silica shells. A combination of these three

parameters will enable and even more drastic expansion of the detection probe library for multiplexing bioassays.

Note that this part of this thesis work is not complete due to time constraint. Synthesis of silica core and shell, and control of shell thickness are characterized and reported in this thesis, but fluorescence labeling to silica shell and encapsulation of various nanomaterials into silica cores are still a work in progress. However, *Chapter 2* successfully demonstrated fluorescence labeling into a silica matrix, and its fluorescence lifetime control and characterization by a phasor method. In parallel, synthesis of QD-encapsulated silica (QD-Si) cores—fluorescent silica shell NPs and their fluorescence lifetime characterization is in investigation by Rajesh Kota, and its progress will be reported in this thesis as an example of the nanomaterial-encapsulated silica cores. With more research and empirical data, this novel core-shell system has a great potential to contribute to multiplexing molecular detection.

3.2 Materials and methods

i) Synthesis of silica core

The fundamental synthesis protocol of silica cores is described by Darbandi *et al.* [29]. 1.3 ml of polyoxyethylene (5) nonylphenylethr (IGEPAL CO-520, Sigma-Aldrich) was added to 10ml of cyclohexane (99%, EMD Millipore) and then mixed vigorously for 15 minutes. While stirring, 100ul of toluene (99.8%, Sigma Aldrich) was added to the solution and mixed for another 15 minutes. The addition of non-polar organic solvent provides this synthesis protocol with a capacity to encapsulate various nanomaterials, such as organic ligand-coated QDs, into silica cores. 80ul of TEOS was then added and mixed for 30 minutes. In order to study the effect of ammonia concentration on the core size, different amounts of ammonia (10ul, 30ul, 75ul,

150ul, and 300ul) were slowly added to the mixture to catalyze the reaction. The solution was then stirred overnight. To ensure colloidal stability of silica cores, 5ul of TEOS and 15ul of 3-(trihydroxysilyl)propyl methylphosphonate, monosodium salt solution (Sigma Aldrich; will be referred to as phosphonate) were added and stirred overnight for particle surface modification. After completing the reaction, the reverse microemulsion was destabilized and its products were isolated by adding ethanol (1:2 volume ratio of ethanol to the reaction mixture), followed by centrifuge and successive washes with ethanol and water to remove the surfactants and any impurities (@ 14000 rpm, 10 min for each wash).

ii) Synthesis of silica shell

Silica shell synthesis was prepared according to the Stober sol-gel method. The washed silica cores from *part i* were suspended in 10ml of ethanol and stirred. While stirring, various amounts of TEOS (2ul, 10ul, 20ul, and 50ul) were then added to create different thicknesses of the silica shell. 150ul of ammonia was added to the reaction and was stirred for 24 hours followed by successive centrifugation and replacement of supernatant with ethanol and water (@ 14000 rpm, 10min for each wash).

iii) Fluorescent labeling of silica shell

Following the same fluorescent dye coupling procedure from *part ii* of chapter *2.2*, NHS-Rhodamine will be coupled with various amounts of APTS and different F:Si molar ratios in ethanol while being stirred in the dark for 24 hours. The volume ratio of APTS to ethanol will be kept consistent to 1:50 throughout the silanization reactions.

While stirring, the Si-F solution and TEOS will be simultaneously added to the washed silica cores suspended in 10ml ethanol. In order to catalyze co-condensation of Si-F into the silica shell matrix, 150ul of ammonia will be added to the reaction. The reaction will then be

stirred for 24 hours followed by successive centrifugation and replacement of supernatant with ethanol and water (@ 14000 rpm, 10 min for each wash).

3.3 Results and discussion

i) Particle synthesis and size analysis

The size of silica cores was analyzed by DLS with the same sample preparation and settings used in *Chapter 2*. In order to study the effect of ammonia concentration on the core size, different amounts of ammonia (10ul, 30ul, 75ul, 150ul, and 300ul) were used in the reactions. The sizes were 353nm, 127nm, 101nm, 35nm, and 34nm for 10ul, 30ul, 75ul, 150ul, and 300ul of ammonia, respectively. The introduction of the catalyst into the microemulsion reaction gives rise to nuclei formation that grows into small particles until all the reactants are used [30]. Therefore, an increase in the amount of ammonia in the reaction system initially gives a rapid rise to the number of nuclei that grow into particles until all TEOS is exhausted. Since the amount of TEOS was kept consistent throughout the experiments, the system with more ammonia had more initial nuclei formation that led to faster exhaustion of reactants, thus the smaller particle size.

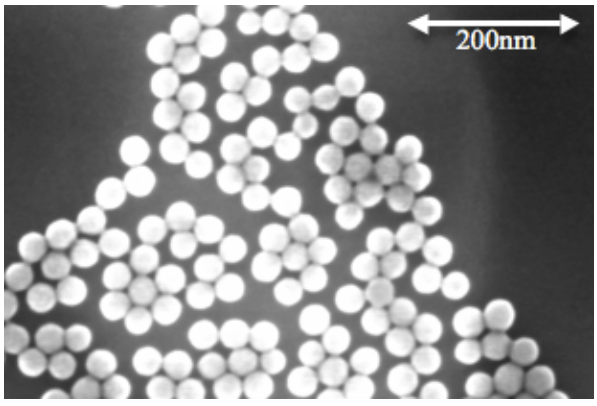

Figure 3 | SEM image of silica cores synthesized with 150ul ammonia.

Ammonia (ul)	Core size (nm)
10	353
30	127
75	101
150	35
300	34

TEOS (ul)	Core-shell NP size (nm)
2	44
10	53
20	69
50	76

Table 2 | The effect of different amounts of ammonia to the size of the silica cores; and the effect of different amounts of TEOS to the size of the core-shell NPs. Note that 80ul of TEOS was kept consistent throughout the ammonia vs. core size experiment; and 150ul of ammonia was kept consistent throughout the TEOS vs. core-shell NP size experiment. Cores with a diameter of 35nm were used for the core-shell NPs.

Silica shells were synthesized to 35nm cores with 150ul of ammonia and different amounts of TEOS to create various thicknesses in the shell. The size of the shell-coated cores was 44nm, 53nm, 69nm, and 76nm for 2ul, 10ul, 20ul, and 50ul of TEOS, respectively. The control over the shell thickness plays an important role in fluorescent labeling of the NPs and engineering their fluorescence intensity. Since a thicker shell has more capacity to hold fluorophores, more fluorescent dye molecules can be incorporated into the shell matrix while minimizing self-quenching.

ii) QD-encapsulated silica (QD-Si) cores—fluorescent silica shell NPs

To demonstrate a theoretical analysis on the fluorescence lifetime of the core-shell NPs, QD-Si cores—fluorescent silica shell NPs were chosen. As demonstrated in *Chapter 2.3*, fluorescently labeled silica shell matrices will follow the same quenching pattern of the matrices

that show an increasing level of quenching and shortening of lifetime as the amount of aminosilane or the F:Si ratios increases (*Figure 2*). In parallel, the fluorescence lifetime of the QD-Si cores can be independently controlled by varying the concentration of QD particles in the silica core matrices.

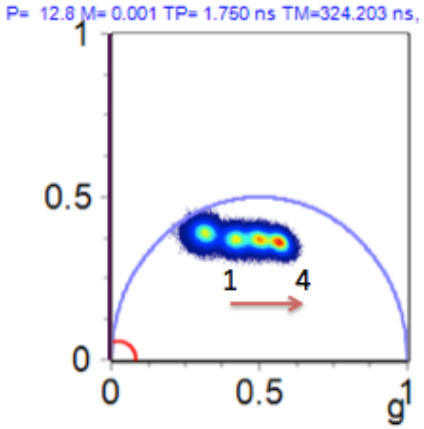

Figure 4 | A phasor plot of the QD-Si cores with various levels of quenching. As the concentration of QD particles used during the core synthesis increased, the phasor values shifted from left to right, indicating that quenching of QD particles had taken place in the silica cores. From the left to the right, the first phasor spot represents the overlapped readings of 0.4mg/ml, 0.8mg/ml, and 1mg/ml samples; the second spot represents 2mg/ml sample; the third spot represents 4mg/ml sample; and the last spot represents the overlapped readings of 8mg/ml and 10mg/ml samples.

The self-quenching of QD particles in the silica cores can be controlled by varying the concentration of QD particles during the silica core synthesis. In Kota's work, the concentrations used in the synthesis solution to manipulate the fluorescence lifetime of the QD particles were 0.4mg, 0.8mg, 1mg, 2mg, 4mg, 8mg, and 10mg QD particles per 1 ml of toluene. The QD particles did not quench up until 1mg/ml, so the samples that used concentrations of 0.4mg/ml, 0.8mg/ml, and 1mg/ml overlapped at the same location on the far left (*Figure 4*). As the concentration increased, their phasor values shifted toward the right, indicating that fluorescence quenching had taken place among the QD particles. However, the cores with a higher QD concentration equal or above 8mg/ml started to saturate and did not shift to the right any further.

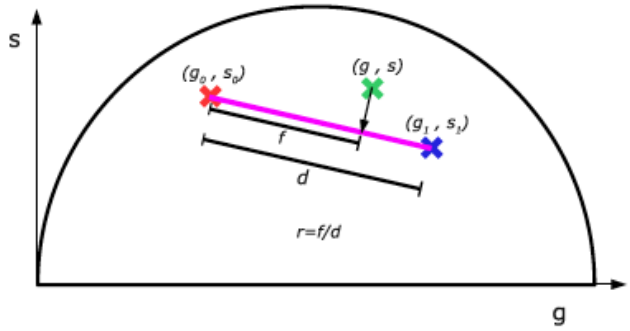

Figure 5 | A schematic of the phasor value (g, s) of a sample containing two fluorescent populations with two different phasor values, (g_0, s_0) and (g_1, s_1) [31].

Since QD-Si core—fluorescent silica shell NPs hold two fluorescent species with two distinct phasor values, the fluorescence lifetime of the core-shell NPs will exhibit unique phasor values produced by the relative contributions of the two species. The combined phasor values (g, s) will show on the line connecting the phasor value of a population (g_0, s_0) and the phasor value of another population (g_1, s_1) (*Figure 5*). The relative contribution in this QD-Si core—fluorescent silica shell NP design is the relative fluorescence intensities of the QD particles in the cores and the fluorescent dye molecules in the shells. The fluorescence intensity will depend on the size of the cores and the thickness of the shells, because increasing the size and the thickness provides the silica matrices more capacity to hold more fluorophores. However, the ratio of the amount of fluorophores to the silica matrix volume has to be taken into consideration, as the intensity may saturate when that ratio reaches above the critical concentration of the fluorophores.

CHAPTER 4. SUMMARY AND CONCLUSIONS

In the first part of this thesis, silica spheres with a diameter of ~130nm were successfully synthesized and fluorescently labeled with Oregon Green, BODIPY, and Rhodamine via the Stober sol-gel synthesis method. The fluorescence quenching was demonstrated in the silica NPs by covalently incorporating Si-F into the silica matrix with different F:Si molar ratios. The intensity-based fluorescence characterization showed that an increase in the fluorophore concentration decreased the relative fluorescence efficiencies, because the energy of the excited fluorophores non-radiatively returns to the ground state due to the fluorescence quenching. The fluorescence lifetime analyses using a phasor approach revealed that higher levels of quenching shortened the fluorescence lifetime and shifted the phasor values toward the right side of the universal circle.

Utilizing the versatile properties of silica, a core-shell NP structure was synthesized consisting of silica cores with a diameter of ~35nm and silica shells with various thicknesses. Although the core-shell NP work is still a work in progress, the application of a core-shell architecture in expanding the molecular probe library through the three main design parameters was explained. The phasor values of the fluorescence lifetimes of the fluorescent silica shell is controlled by covalently incorporating Si-F into the silica matrix with different amounts of aminosilane and F:Si molar ratios, as demonstrated in *Chapter 2*. The thickness of the shell enables the control over the fluorescence intensity of the shell. Meanwhile, the phasor value of the silica core is independently controlled by the quenching among the nanomaterials encapsulated in the cores. As an example, the QD-Si cores were chosen to illustrate how various concentrations of the QD NPs, or the various levels of quenching among the QD NPs, affect

shifting in the phasor values of the cores. A core-shell silica NP architecture with an independent control for the fluorescence lifetimes of the core and shell, and an ability to vary fluorescence intensity through the shell thicknesses creates a complex system that can drastically extend the number of the detection channels.

This thesis has successfully demonstrated that the particles with the same excitation and emission wavelengths can exhibit various fluorescence lifetimes through a phasor approach to fluorescence lifetime by manipulating the molecular proximity of fluorophores and the non-radiative process of self-quenching. Distinct fluorescence lifetime phasor values enable silica NPs to have visually effective representations of fluorescence lifetime that are unique and distinguishable. Due to the synthetic versatile properties in accommodating foreign materials, the core-shell structured silica NPs with multiple fluorescent materials were discussed that can open the door to an exponential rise in the number of molecular probes using a phasor approach to fluorescence lifetime.

REFERENCES

[1] Cooper, G. and Hausman, R. The Development and Causes of Cancer. *The Cell: A Molecular Approach*, 2nd ed. **2000**.

[2] Fuster, J., Fernandez, P., Gonzalez-Navarro, H. , Silvestre, C., Naban Y., and Andres, V. Control of cell proliferation in atherosclerosis: insights from animal models and human studies. *Cardivascular Research* **2010**; 86 (2), 254-264.

[3] Ledzewicz, U. and Schattler, H. On optimal chemotherapy for heterogeneous tumors. *Journal of Biological Systems* **2014**; 22 (2), 177-197.

[4] Davis, E., Chen, G., and Shin, M. Nature Reviews Drug Discovery **2008**; 7, 771-782.

[5] Liong, M., Lu, J., Kovochich, M., Xia, T., Ruehm S., Nel, A., Tamanoi, F., and Zink, J. Multifunctional inorganic nanoparticles for imaging, targeting, and drug delivery. *ACS Nano* **2008**; 2 (5), 889-896.

[6] Singh, R., and Lillard, J. W., Jr. Nanoparticle-based targeted drug delivery. *Exp. Mol. Pathol*. **2009**; 86 (3), 215-223.

[7] Ge H., Hu Y., Jiang X., Cheng D., Yuan Y., Bi H., and Yang C. J. Preparation, characterization, and drug release behaviors of drug nimodipine-loaded poly(epsilon-caprolactone)-poly(ethylene oxide)-poly(epsilon-caprolactone) amphiphilic triblock copolymer micelles. *Pharm Sci.* **2002**; 91(6), 1463-73.

[8] Villaverde, A. Progress in molecular biology and transitional science. *Elsevier* **2011**; 104, 1-615.

[9] Algar, R., Prasuhn, E., Stewart, M., Jennings, L., Blanco- Canosa, B., Dawson, E., and Medintz, L. The controlled display of biomolecules on nanoparticles: a challenge suited to bioorthogonal chemistry. *Bioconjugate Chem.* **2011**; 22, 825-858.

[10] Li, S.D. and Huang. L. Pharmacokinetics and biodistribution of nanoparticles. *Molecular Pharmaceutics* **2008**; 5 (4), 495-504.

[11] Barbé, C., Bartlett, J., Kong, L., Finnie, K., Lin H. Q., Larkin, M., Calleja, S., Bush, A., and Calleja, G. Silica Particles: A Novel Drug-Delivery System. *Advanced Materials* **2004**; 16 (20), 1959-1966.

[12] Reddy, L. H., Arias, J. L., Nicolas, J., and Couvreur, P. Magnetic nanoparticles: Design and characterization, toxicity and biocompatibility, pharmaceutical and biomedical applications. *Chem. Reviews* **2012**; 112 (11), 5818.

[13] Wise, D. L. Handbook of pharmaceutical controlled release technology. *Marcel Dekker*: New York **2000**.

[14] Li, X., Wang, L., Fan, Y., Feng, Q., and Cui, F. Biocompatibility and toxicity of nanoparticles and nanotubes. *Journals of Nanomaterials* **2012**; 2012.

[15] Knezevic, N. Z., and Durand, J. Targeted treatment of cancer with nanotherapeutics based on mesoporous silica nanoparticles. *ChemPlusChem*. **2015**; 80 (1), 26-36, 11p.

[16] Ma, Y., Li, Y., and Zhong, X. Silica coating of luminescent quantum dots prepared in aqueous media for cellular labeling. *Materials Research Bulletin* **2014**; 60, 543-551.

[17] Diebold, E. D., Buckley, B. W., Gossett, D. R., and Jalali B. Digitally synthesized beat frequency multiplexing for sub-millisecond fluorescence microscopy. *Nature Photonics* **2013**; 7 (10), 806-810.

[18] Stober, W., and Fink, A. Controlled growth of monodisperse silica spheres in the micron size range. *Journal of Colloid and Interface Science* **1968**; 26, 62-69.

[19] Bogush, G. H., Tracy, M. A., and Zukoski, C. F. Preparation of monodisperse silica particles: Control of size and mass fraction. *Journal of Non-Crystalline Solids* **1988**; 104 (1), 95-106.

[20] Haun, J. B., Robbins, G. P., and Hammer, D. A. Engineering therapeutic nanocarriers with optimal adhesion for targeting. *The Journal of Adhesion* **2010**; 86, 131-159.

[21] Lakowicz, J. R. Principles of fluorescence spectroscopy. *Springer*: New York **2006**.

[22] Zeng, L. Developing a mesoporous silica nanoparticle platform for optimizing adhesion of targeted therapies (Master's thesis). *ProQuest.UMI* **2013**; (Accession No. 1541069).

[23] Zhao, X., Bagwe, R. P., and Tan, W. Development of organic-dye-doped silica nanoparticles in a reserve microemulsion. *Advanced Materials* **2004**; 16 (2).

[24] Wang, L., and Tan, W. Multicolor FRET silica nanoparticles by single wavelength excitation. *Nano Letters* **2005**; 6 (1), 84-88.

[25] Sauer, M., Hofkens, J., and Enderlein, J. Handbook of fluorescence spectroscopy and imaging. *Wiley-VCH*: Weinheim **2011**.

[26] Kasha, M., Rawls, H. R., El-Bayoumi, M. A. Excitation model in molecular spectroscopy. *Pure Appl. Chem.* **1965**; 11, 371-392.

[27] Vogt, C., Toprak, M. S., Muhammed, M., Laurent, S., Bridot, J., and Muller, R. N. High quality and tuneable silica shell-magnetic core nanoparticles. *Journal of Nanoparticle Research* **2010**; 12 (4), 1137-1147.

[28] Nghiem, Thi Ha Lien, Le, Tuyet Ngan, Do, Thi Hue, Vu, Thi Thuy Duong, Do, Quang Hoa, and Tran, Hong Nhung. Preparation and characterization of silica-gold core-shell nanoparticles. *Journal of Nanoparticle Research* **2013**; 15 (11), 1-9.

[29] Darbandi, M., Thomann, R., and Nann, T. Single quantum dots in silica spheres by microemulsion synthesis. *Chem. Mater.* **2005**; 17, 5720-5725.

[30] M. A. Lopez-Quintela, J. Rivas, M. C. Blanco, and C. Tojo. Synthesis of nanoparticles in microemulsions. *Nanoscale Materials* **2003**; 135-155.

[31] Colyer, R., Siegmund, O., Tremsin, A., Vallerga, J., Weiss, S., and Michalet, X. Phasor imaging with a widefield photon-counting detector. *Journal of Biomedical Optics* **2012**; 17 (1), 016008.

[32] Lee, C., and Hua, C. Fundamental pair interactions and applications for colloidal silica particles by coarse-grained simulations. *AIP Conference Proceedings* **2008**; 1027 (1); 707-709.

APPENDIX

The calculation for NP concentration was based on assumptions that 1) the reaction of all TEOS molecules had gone to completion for particle nucleation and that 2) a density of silica NPs are 2.2g/cm^3 [32]. 500ul of TEOS was used for the NP synthesis, so the total mass of TEOS is,

$$500ulTEOS * (\frac{ml}{1000ul}) * (\frac{0.933g}{ml})$$

where 0.933g/ml is the density of TEOS. Since the NP is a sphere and its diameter is ~130nm, the mass of a NP can be calculated by using the given density of silica NP.

$$\frac{4}{3} * (65 * 10^{-7})^3 * 2.2\frac{g}{cm^2}$$

When the total mass of TEOS is divided by the mass of a NP, the total number of NPs synthesized from 100ul of TEOS is 1.8 X 10^{14}. Then the final NP concentration of 0.3nM was calculated using Avogadro's number.